Nuclear Instruments and Methods in Physics Research B 268 (2010) 2446–2450

Contents lists available at ScienceDirect

Nuclear Instruments and Methods in Physics Research B

journal homepage: www.elsevier.com/locate/nimb

Digitized neutron imaging with high spatial resolution at a low power research reactor: Applications to steel and rock samples

M. Zawisky [a,*], F. Hameed [a], E. Dyrnjaja [a], J. Springer [a], A. Rohatsch [b]

[a] Vienna University of Technology, Atomic Institute, Vienna, Austria
[b] Vienna University of Technology, Institute for Engineering Geology, Vienna, Austria

ARTICLE INFO

Article history:
Received 28 January 2010
Received in revised form 19 April 2010
Available online 27 April 2010

Keywords:
Neutron imaging
Neutron tomography
Transmission analysis
Boron alloyed steel
Non-destructive measurements
Feldspar

ABSTRACT

Improved spatial detector resolution is exploited for engineering and geology, e.g., for the investigation of boron distribution in steel, consolidated aspects of building materials, and grain analysis in feldspar. The strengths and limitations of the upgraded instrument are evaluated in the context of these projects. First promising results have been obtained and will extend the range of applications for the neutron imaging beam-line at the Atomic Institute in Vienna.

1. Introduction

The development of neutron imaging techniques has a long tradition at the Atomic Institute operating a 250 kW TRIGA MARK II reactor located in Vienna, Austria [1–4]. Digitized imaging with 16 bit full dynamic range and high spatial resolution are key features of a state-of-the-art neutron radiography (NR) and neutron tomography (NT) instrument. A major instrument upgrading was required in order to meet the partners' demands [5]. In this article current projects are presented where an improved detector resolution and image gradation are of great value.

The first project concerns the investigation of boron alloyed steels to be used as neutron shielding in nuclear engineering. The goal is the evaluation of uniform ^{10}B distribution and the transmission behavior. The measurements are assisted by Monte Carlo simulations in order to analyze the effect of micro-heterogeneities on neutron transmission. A second main field of application for this instrument is sensitive detection of hydrogen in rocks and building materials for geological investigations and the assessment of consolidation procedures. Improvements in hydrogen detection, better spatial resolution and finer image gradation are presented.

2. Investigation of boron alloyed steels

Boron alloyed steel sheets are used as neutron shielding for radioactive waste disposal equipment, e.g., compact fuel racks for the intermediate storage of spent fuel elements where criticality accidents have to be ruled out by sufficient absorption capacity in the steels, and for transportation casks. The NR facility benefits from a well defined thermalized neutron spectrum with Maxwellian energy distribution which is close to the neutron field under realistic conditions, when spent fuel rods are stored in a water tank [6–8]. The boron alloyed steels are manufactured by Böhler Bleche GmbH, Mürzzuschlag in Austria, with dimensions of several square meters; the neutron attenuation is tested at the companies' site by scanning a mobile ^{252}Cf source across selected positions of the surface with 100 cm^2 resolution [8]. Small pieces are provided by the manufacturer and further machined at the Atomic Institute to sheets with identical thickness and good surface quality. The goal of this project is the verification of uniform boron distribution to evaluate the melting and milling processes and the quantification of neutron attenuation.

At first, 18 steel sheets with 0.137 cm thickness have been investigated individually using NR imaging with high spatial resolution. The nominal boron content in this measurement series was 1.88 wt.% (0.35 wt.% ^{10}B). Within the scintillator's resolution no statistically significant regions of reduced boron were found, a selected sample is shown in Fig. 1. The variance of pixel counts δN was less than $3 \times \sqrt{N_{\text{average}}}$ for all sheets.

* Corresponding author. Address: Vienna University of Technology, Atomic Institute, Stadionallee 2, 1020 Vienna, Austria. Tel.: +43 1 58801 14170; fax: +43 1 58801 14199.
E-mail address: zawisky@ati.ac.at (M. Zawisky).

0168-583X/$ - see front matter © 2010 Elsevier B.V. All rights reserved.
doi:10.1016/j.nimb.2010.04.020

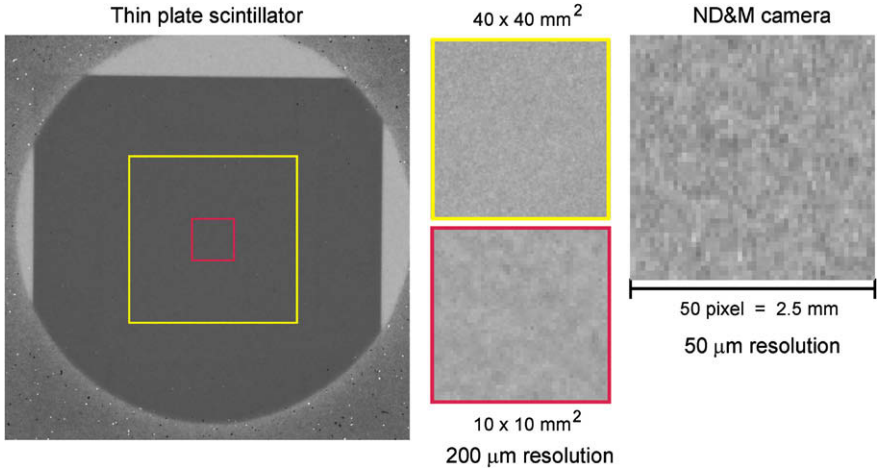

Fig. 1. Transmission images of a 0.137 cm thick boron alloyed steel plate. The variance of pixel counts δN is $2.3 \times \sqrt{N_{\text{average}}}$ in the scintillator, and $1.2 \times \sqrt{N_{\text{average}}}$ in the ND&M [5] detector pixels. The maximum intensity contrast $(I_{\max} - I_{\min})/(I_{\max} + I_{\min}) = 23\%$ in the ND&M pixel counts.

The homogeneity measurements were repeated with the new imaging plate detector (NIP) using the BAS-5000 readout scanner with 25 μm nominal resolution. The plates were placed directly in front of the NIP with 40 μm vertical and 60 μm horizontal effective resolutions. Unfortunately, the NIP's intrinsic granular microstructure complicates the analysis of absorber inhomogeneities [5]. To correct for the granularity, the plate has to be adjusted in exactly the same position for open beam correction (Eq. (1)). This was accomplished by overlapping three or more dark pixel areas which appear in contrast enhanced sample and open beam images as well (Fig. 2). Again, no significant boron inhomogeneities were found in the steel plates.

Finally, steel sheets with the same composition and thickness have been combined to stacks of larger thicknesses for transmission analysis (Fig. 3). The transmission was averaged in an area of 1 cm^2 to reduce statistical uncertainties:

$$T = \frac{N_s - N_b}{N_o - N_b} \tag{1}$$

N_s and N_o are the counts behind the sample and in the open beam, respectively, and N_b represents the background. N_b has a great effect on low transmission experiments when N_s approaches N_b; it depends mainly on detector noise [5,9] and scattered neutrons which reach the detector without passing the sample. Therefore all critical parts have been shielded with a polyethylene-based shielding material (borolene) with 10 wt.% boron. The sample was masked with 2.5 cm thick borolene in order to guarantee that all detected neutrons pass the 1 cm^2 sample area. The transmission has been calculated according to Eq. (1) where N_b represents the background by closing the open mask area with 10 cm thick borolene. The neutron intensity surrounding the mask was confirmed to be uniform and reached the background level with closed mask. This confirms that backscattered neutrons have no influence on the transmission measurements using the setup shown in Fig. 3.

Because of the exponential nature of the absorption law, particle density fluctuations (δN) to smaller densities have a greater effect than to higher densities, and the transmission becomes larger [10]. Every neutron track through the steel experiences a slightly different amount of boron, and Monte Carlo simulations (MCNPX 2.4.0, Los Alamos National Laboratory) are able to deliver an averaged transmission of a large number of stochastic neutron tracks considering the neutron spectrum, multiple scattering and absorption probabilities of the ^{6}Li scintillator and the imaging plate [5]. Simulations with non-homogeneous models always yield enhanced neutron transmission. In Fig. 3 different MCNPX models are compared, the homogeneous case where boron is distributed uniformly in the whole volume, and a hexagonal lattice model where all boron is concentrated in globules, alloys of boron and steel, centered in steel cells (Fig. 4). The total amount of boron has been preserved in all simulations. For a better definition of the structure sizes, steel investigations have been performed at the ultra-small angle (USANS) instrument of the Atomic Institute indicating an average grain radius (R) of the ferro-borides of approx. 11 μm. For such a micro-structure it was possible with

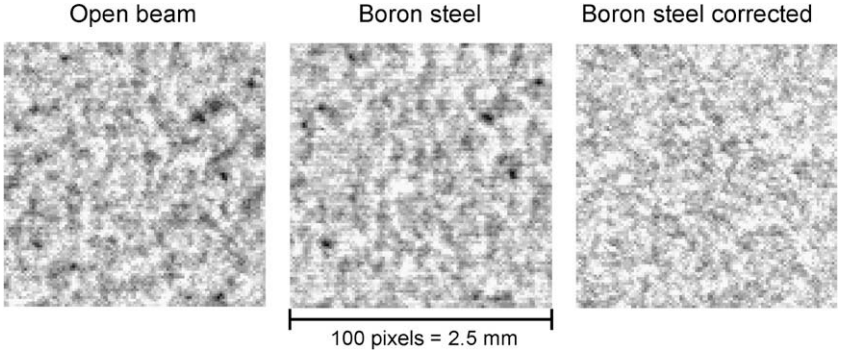

Fig. 2. Steel inspection with the neutron imaging plate detector. The search for inhomogeneities in boron alloyed steels is complicated by the intrinsic granular structure of the NIP (left). The transmission image of the steel is superimposed by the NIP's granularity (middle). After open beam correction (right) no significant inhomogeneities remained: $(I_{\max} - I_{\min})/(I_{\max} + I_{\min}) = 10\%$ (images contrast enhanced only for presentation).

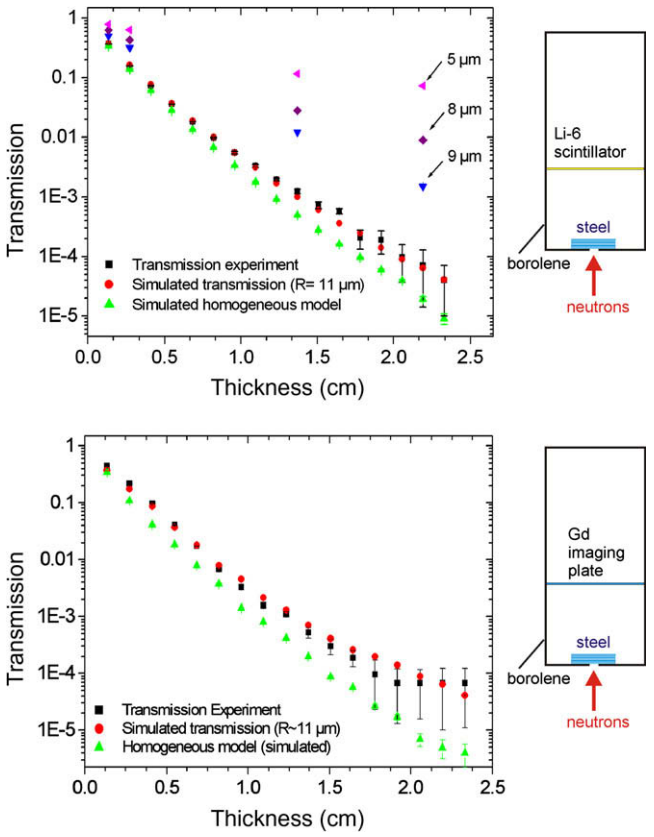

Fig. 3. Neutron transmission in strong absorbing steels with $\Sigma = 7.5/\text{cm}$ macroscopic attenuation cross section compared with different MCNPX models. By increasing the boron spheres (R = average grain radius) one approaches the homogeneous model, contrary, by reducing the globule size the transmission becomes enhanced (top). A slightly enhanced transmission was observed with both detectors (top: 100 μm thick scintillation plate, bottom: imaging plate) due to micro-inhomogeneities of the boron distribution in the steel.

MCNPX to describe the transmission experiment shown in Fig. 3 thereby revealing a slightly enhanced neutron transmission compared to the homogeneous model.

3. Applications in geology and consolidated aspects of building materials

Recently, investigations in engineering geology have been started at the Atomic Institute, aiming at the assessment of chemical restoration work in historical buildings [11], the study of grain sizes and distributions, and the intergrowth with other minerals in stones. Good spatial resolution and high detection sensitivity for hydrogen and rare earth elements are the basis for these projects [12]. Fig. 5 shows a parallel cut feldspar, with 35 mm thickness and two plane surfaces, directly placed in front of the detector. The comparison emphasizes the supremacy of the NIP particularly in comparison with a conventional Gd-film detector using a 25 μm gadolinium foil as converter and an X-ray film (Structurix D7).

Typically, 200 projections are used in the angular range 0°–180° for a tomography yielding a total measurement time of 11 h with the new 100 μm scintillator. The number of projections and measurement time could further be extended to exhaust the full dynamic range of the CCD chip. IDL (ITT Visual Information Solutions, [13]) and Octopus software (University Ghent, Belgium, [14]) is implemented for tomographic reconstruction, and VGStudio (Volume Graphics GmbH, [15]) for 3D rendering.

Fig. 6 shows a typical lime-sandstone, as used in Viennese churches and sculptures, it was chemically consolidated with an acrylic resin and five months later analyzed with neutrons. The goal of this project is to investigate the penetration and distribution of different consolidation agents in lime-sandstones used for the restoration of sculptures and historical buildings [11]. Neutron tomography is indispensable for a complete assessment of the chemical restoration procedure, in particular for the categorization of surface and volume effects. The stone was consolidated from the bottom in a soaking bath with 1 cm depth, therefore, a rather homogeneous distribution of the consolidant was expected up to a height of 2–3 cm. However, tomography revealed a pronounced surface effect, where the consolidant (red colored regions) was preferably distributed along the surface up to 4 cm in height.

Fig. 7 shows a quartz sandstone from the façade of a monastery in Salzburg, 18th century. The stone was treated with ethyl silicate consolidant by the floating method from the outer surface, as marked in the photograph (Fig. 7, left). Ideally, the consolidants should form a silica gel ($SiO_2{\cdot}xH_2O$) and be homogeneously distributed up to 1–2 cm depth. According to the neutron tomography, the consolidants have reached the expected depth but are not uniformly distributed. The red segments represent regions of higher neutron attenuation due to the water content in the gel. A maximum difference in neutron attenuation of 14% has been derived from the sample shown in Fig. 7.

4. Hydrogen detection sensitivity in thin materials

In thin wetted slices the beam attenuation can be described by Eq. (2) using the total macroscopic cross section $\Sigma = \Sigma_a + \Sigma_s$

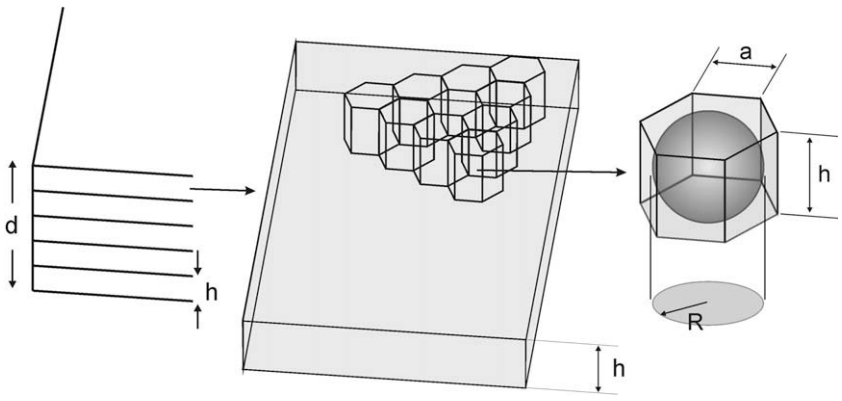

Fig. 4. In this MCNP model boron is concentrated in spheres centered in hexagonal cells. The steel is composed of several layers of cells with height h. Good agreement with transmission data was obtained with following parameters: R = 11 μm, a = 10 μm, h = 20 μm, d = total sheet thickness.

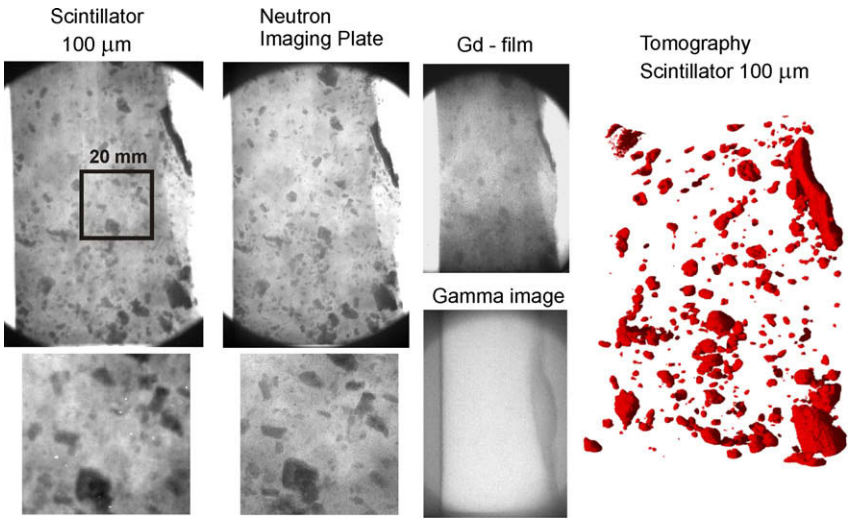

Fig. 5. Neutron images of a 35 mm thick feldspar reveal dark regions of boron (3.3%) in tourmaline, hydrogen in muscovite (mica), and spurious rare earth elements in garnet. The unprocessed images demonstrate the hierarchy of detector resolution, the best result with the NIP (10 min exposure). The gamma image was taken with a X-ray sensitive imaging plate. In the tomography a 3D analysis yields 343 grains with a mean grain volume of 2.8 mm^3 and a grain/stone volume (porosity) of 1.3%.

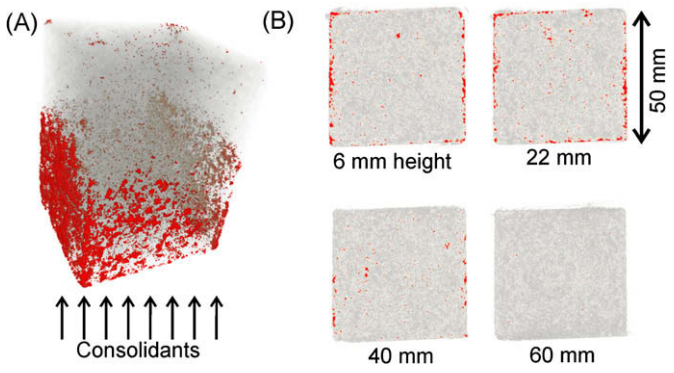

Fig. 6. Neutron tomography of restoration agents (red regions) in a calcareous arenite. (A) Surprisingly, the agent is preferably distributed near the surface up to 4 cm height (100 μm scintillator). (B) Slices in different heights from the bottom.

($\Sigma_{a,s}$ = absorption, scattering cross sections). Fig. 8 shows a thin calcareous arenite with $d = 4$ mm. From the measured hydrogen density one derives a mean path length of 40 mm hence multiple scattering remains negligible in wetted thin-slices [16,17]. Empirically, by changing the sample-to-detector distances from 2 to 29 cm, no scattering artifacts have been found in wetted slices up to 4 mm thickness. A statistical limit for density resolution $\Delta\rho$ in small sample areas can be derived from the variance of pixel count numbers (δN) in the area of interest [18]:

$$T_{\text{water}} \cong \frac{N_{\text{wet}}}{N_{\text{dry}}} \cong e^{-\Sigma d} = \exp\left(-\frac{\rho\sigma N_A d}{M}\right) \tag{2a}$$

$$\Delta\rho_{\text{water}} \cong \sqrt{\left(\frac{\delta N_{\text{wet}}}{N_{\text{wet}}}\right)^2 + \left(\frac{\delta N_{\text{dry}}}{N_{\text{dry}}}\right)^2}\,\frac{M}{d\sigma N_A} \tag{2b}$$

Here, N_{wet}, N_{dry} represent the total count numbers of the wet and dry samples in the area of interest, σ denotes the microscopic cross section of water, M the molecular weight and N_A the Avogadro constant.

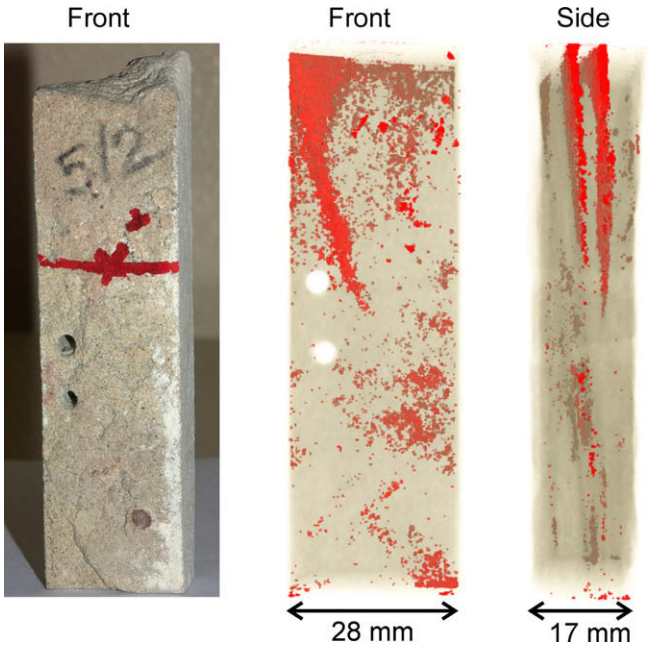

Fig. 7. Tomography of a quartz sandstone from the façade of a monastery in Salzburg. The red segments highlight regions of higher neutron attenuation caused by the consolidants and stone compaction.

In order to determine the sensitivity to hydrogen detection an aluminum vessel with adjustable thickness, filled with light water, has been prepared. Fig. 9 shows a 40 μm water film, whereby the wet sample image is normalized to the dry image for determining the water density. The statistical density resolution yields $\Delta\rho \approx 0.03$ g/cm^3 in areas of 1 mm^2 along the black line by exploiting the full 16 bit dynamic range, i.e., 50 min exposure time at 25 μm pixel resolution.

5. Summary

Boron alloyed steel sheets have been investigated by applying neutron radiography inspection with high spatial resolution. A

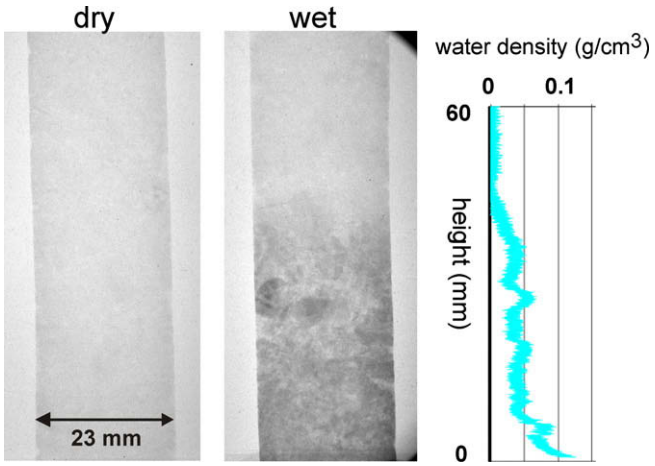

Fig. 8. NIP images of a 4 mm thin-slice calcareous arenite in dry and wet condition after 30 min wetting in a soaking bath. Density fluctuations due to inhomogeneous hydrogen distribution are recorded along the vertical axis in steps of 25 μm.

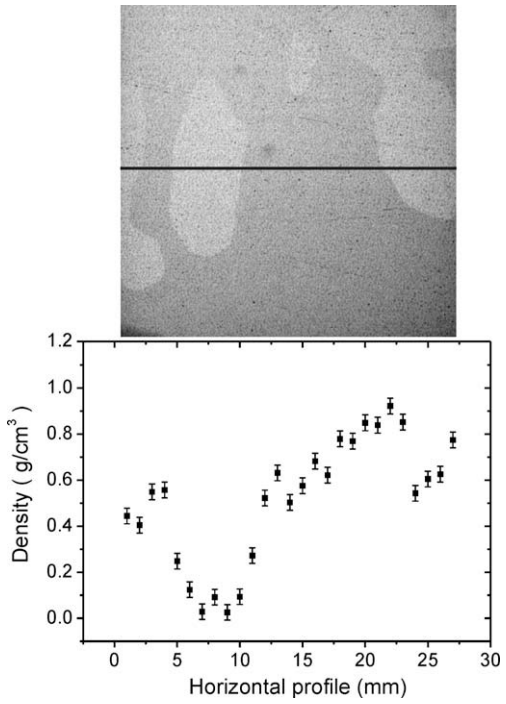

Fig. 9. Analysis of a 40 μm inhomogeneous water layer using an imaging plate with 25×25 μm^2 readout resolution. Regions of different water content are clearly resolved (contrast of raw images enhanced for presentation).

high degree of homogeneity of the boron distribution has been confirmed in thin sheets. However, the transmission analysis of thicker steel sheets, accompanied by MCNPX simulations, revealed a slightly enhanced average transmission due to micro-inhomogeneities of the boron in the range of 20 microns.

Neutron tomography facilitates the assessment of chemical restoration work in building materials, e.g., to distinguish between surface and volume effects. The method has also been used to study grain sizes and distributions in feldspar. Finally, the high neutron sensitivity to hydrogen was applied to thin wetted calcareous arenites and thin water films. Density resolution of the order of 0.02 g/cm^3 could be achieved in small sample regions by exploiting the full dynamic range of the new scintillation and imaging plate detectors.

Acknowledgements

We would like to thank BÖHLER Bleche GmbH, Mürzzuschlag in Austria for providing the boron alloyed steel sheets, E. Jericha (Atomic Institute) for performing USANS measurements on the steels, and B. Grasemann, U. Exner and M. Edwards, University of Vienna, for providing geological samples and chemical analysis.

References

[1] H. Rauch, A. Zeilinger, At. Energ. Rev. 15 (2) (1977) 249.
[2] C. Degueldre, H. Pleinert, P. Maguire, E. Lehmann, J. Missimer, J. Hammer, K. Leenders, H. Böck, D. Townsend, Earth Planet. Sci. Lett. 140 (1996) 213.
[3] M. Bastürk, M. Bichler, A. Dlouhy, B. Zamani, M. Zawisky, In: Proc. 16th World Conference on NDT, NDT.NET vol. 9, no. 11, Montreal, Canada, 2004.
[4] M. Bastürk, H. Böck, B. Zamani, M. Zawisky, H. Rauch, In: Proc. 2nd TRIGA Users Conference, Vienna, Austria, 2004, pp. 8.
[5] M. Zawisky, F. Hameed, E. Dyrnjaja, J. Springer, Nucl. Instrum. Meth. A 587 (2008) 342.
[6] M. Zawisky, M. Bastürk, R. Derntl, F. Dubus, E. Lehmann, P. Vontobel, Appl. Radiat. Isot. 61 (2004) 517.
[7] M. Zawisky, M. Bastürk, J. Rehacek, Z. Hradil, J. Nucl. Mater. 327 (2004) 188.
[8] M. Bastürk, J. Arztmann, W. Jerlich, N. Kardjilov, E. Lehmann, M. Zawisky, J. Nucl. Mater. 341 (2005) 189.
[9] Y. Karasawa Haga, S. Kumazawa, N. Nimura, J. Appl. Cryst. 32 (1999) 878.
[10] H. Rauch, M. Zawisky, Ch. Stellmach, P. Geltenport, Phys. Rev. Lett. 83 (1999) 4955.
[11] F. Hameed, A. Rohatsch, J. Weber, B. Zamani, M. Zawisky, in: M. Arif, R.G. Downing (Eds.), Neutron Radiography 8 – WCNR8, DES Publications, Lancaster, 2008. pp. 251–263.
[12] B. Winkler, K. Knorr, A. Kahle, P. Vontobel, E. Lehmann, B. Hennion, G. Bayon, Eur. J. Mineral. 14 (2002) 349.
[13] IDL software: http://www.ittvis.com/ProductServices/IDL.aspx.
[14] M. Dierick, B. Masschaele, L. Van Hoorebeke, Meas. Sci. Technol. 15 (2004) 1366.
[15] VGStudio MAX: http://www.volumegraphics.com/products/vgstudiomax/.
[16] V.F. Sears, Adv. Phys. 24 (1975) 1.
[17] R. Hassanein, H.O. Meyer, A. Carminati, M. Estermann, E. Lehmann, P. Vontobel, J. Phys. D39 (2006) 4284.
[18] V.F. Sears, Nucl. Instrum. Meth. 213 (1983) 561.